Efficient gene delivery by sonoporation is associated with microbubble entry into cells and the clathrin-dependent endocytosis pathway

Anthony Delalande, Chloe Leduc, Patrick Midoux, Michiel Postema, Chantal Pichon

Title: Efficient gene delivery by sonoporation is associated with microbubble entry to cells and the clathrin-dependent endocytosis pathway.

Authors: Anthony Delalande[1*], Chloé Leduc[1], Patrick Midoux[1], Michiel Postema[2,3], Chantal Pichon[1*].

Affiliations:

1. Centre de Biophysique Moléculaire, CNRS UPR4301, Orléans, France,

2. Department of Physics and Technology, University of Bergen, Bergen, Norway

3. Department of Physics, University of the Witwatersrand, Johannesburg, South Africa.

*: co-corresponding authors: anthony.delalande@cnrs-orleans.fr and chantal.pichon@cnrs-orleans.fr

Abstract

Microbubble oscillation under specific ultrasound settings leads to a permeabilization of surrounding cells. This phenomenon, referred as sonoporation, allows for the *in-vitro* and *in-vivo* delivery of extracellular molecules including plasmid DNA (pDNA). To date, the biological and physical mechanisms behind this phenomenon are still not fully understood. This study aims at investigating the interactions between microbubbles and cells as well as the intracellular routing of pDNA and microbubbles during and post-sonoporation. Investigations were done by high-speed imaging and fluorescence confocal microscopy using HeLa cells stably expressing eGFP fused with markers of cellular compartments. Soft-shelled microbubbles were observed to enter into cells during sonoporation using experimented parameters that led to an optimal gene transfer. They interacted with the plasma membrane in a specific area stained with fluorescent cholera subunit B, a marker of lipid rafts. This process was not observed with hard-shelled microbubbles which were not efficient for gene delivery under our conditions. The pDNA was delivered in late endosomes after 3 hours post-sonoporation and few of them were found in the nucleus after 6 hours. The gene transfer efficacy was greatly inhibited when cells were treated with chlorpromazine, an inhibitor of the clathrin-dependent endocytosis pathway. By contrast, no significant alteration was obtained when cells were treated with Filipin III or Genistein both inhibitors of the caveolin-dependent pathway. This study highlights that microbubble-cell interactions do not occur randomly during sonoporation; microbubbles penetration inside cells imparts the efficacy of gene transfer at specific ultrasound settings and the pDNA uptake is an active mechanism that involves the clathrin-dependent pathway.

Keywords: ultrasound; microbubble; sonoporation; gene delivery; endocytosis; clathrin-mediated endocytosis pathway

Introduction

Although being less efficient than gene delivery by viral vectors; non-viral gene transfer still offers a great promise for gene therapy because of its safety compared to its viral counterparts. Almost twenty years ago, an original drug/gene delivery method based on ultrasound stimulation coupled to gaseous microbubbles was proposed (Bao *et al.*, 1997). Upon ultrasound exposure, microbubbles can oscillate, move, coalesce, fragment, or be disrupted otherwise (Postema and Gilja, 2007). These properties modify the cell membrane permeability by a process known as sonoporation (Bao *et al.*, 1997; Miller *et al.*, 1999; Taniyama *et al.*, 2002). It offers the opportunity of site-specific local delivery of a drug or gene. In the field of gene transfer, several studies have reported an improvement of gene delivery efficacy by sonoporation (Bao *et al.*, 1997; Wang *et al.*, 2005). Numerous *in-vitro* and *in-vivo* studies on sonoporation and its exploitation for gene transfer have been published (Delalande *et al.*, 2011; Delalande *et al.*, 2013; Mehier-Humbert *et al.*, 2005; Noble *et al.*, 2013; Pichon *et al.*, 2008). The main hypothesis assumes a direct entry of the molecules through transient pores in the plasma membrane as a consequence of interaction of oscillating microbubbles with the plasma membrane (Mehier-Humbert *et al.*, 2005; Miller *et al.*, 1999; Taniyama *et al.*, 2002). Transient pores formed at the plasma membrane are responsible for the direct intracellular delivery of small molecules but also the outward transport of intracellular molecules (Kaddur *et al.*, 2010). According to Zhou *et al.,* the pore formed during sonoporation is estimated to be 100 nm wide and opened during 5 seconds (Zhou *et al.*, 2009). The pore formation may be the trigger of many intracellular mechanisms (Juffermans *et al.*, 2009). Several mechanisms of pore membrane formation could occur during sonoporation (for a review see Delalande *et al.* (2012)). However, the mechanisms of

gene transfer from microbubble stimulation, its interaction with cells to gene expression are still not well understood. Recently, some studies have shown that endocytosis process could be involved in the sonoporation mechanism for large molecules (Meijering *et al.*, 2009; Paula *et al.*, 2011), intracellular delivery of liposomes (Afadzi *et al.*, 2013) and lipoplexes (Kurosaki *et al.*, 2014). As pDNA are big molecules over 3 MDa, we suppose that endocytosis should be involved in gene transfer by sonoporation. None of those studies have delineated the complete the process of sonoporation. A better knowledge of the key steps occurring during and after sonoporation could allow for an improvement of this method.

This is the first study making a correlation between optimal ultrasound parameters determination for efficient gene transfer *in vitro* and the processes that govern this efficacy. We observed that under optimal ultrasound parameters that lead to gene transfer, microbubbles interacted preferentially with lipid raft areas of the cell and some of them were found inside cells. Sonoporation-induced gene transfer is not a purely mechanical process but biological as well. Here, we focused on the role of endocytosis in cellular gene uptake. This hypothesis has been confirmed by the use of a clathrin-dependent endocytosis inhibitor that abolished gene transfer efficacy. The plasmid DNA was followed in the cell and was found mainly routed to rab7 positive endosomes 3 hours after sonoporation and close to the nucleus after 6 hours.

Materials and Methods

Cell culture

Human epithelial cervix adenocarcinoma HeLa cells were used in this study (CCL2, ATCC, Rockville, MD). HeLa cells stably expressing the fusion protein Rab7-GFP and Nup153-GFP were developed to localize the fluorescent-labelled pDNA into specific cellular structures (late endosomes and nucleus respectively). HeLa cells were grown in MEM with Earl's salts medium (PAA Laboratories GmbH, Pashing, Austria) supplemented with 10% v/v of FCS and 1% of non-essential amino acids (PAA), penicillin (100 U/mL) and streptomycin (100 µg/mL) at 37°C in a humidified atmosphere containing 5% CO_2. To select Rab7-eGFP and Nup153-eGFP transgene expressing HeLa cells, cell medium was supplemented with G418 (200 µg/mL, PAA). Cells were free from mycoplasma as evidenced by MycoAlert® Mycoplasma Detection Kit (Lonza, Levallois Perret, France).

Plasmid DNA preparation and labelling

A 7.5-kb homemade reporter plasmid that encoded the firefly luciferase gene (pLuc) under the control of the strong cytomegalovirus promoter was used. Five consecutive NFκB motifs that recognized the NFκB transcription factor were inserted upstream of the promoter. All plasmids vectors were propagated from *Escherichia coli* DH5α cultures. Supercoiled plasmid was isolated from bacteria by the standard alkaline lysis method, and purification was carried out with the Qiagen Mega Kit (Qiagen, Courtabœuf, France) according to the manufacturer's instructions. Each pDNA was labelled with the Label IT nucleic acid labelling kit (Mirus, Madison, WI, USA) at 1:2 reagent/pDNA weight ratios according to manufacturer's instructions. When indicated, plasmids were labelled with cyanine 3 or cyanine 5 fluorescein probes followed by

ethanol precipitation for DNA purification. The labelling densities were determined by spectroscopy according to the manufacturer's protocol and corresponded to approximately 1 fluorophore per 80 base pair. We verified that the labelling process of the plasmid did not affect the gene expression.

Ultrasound exposure system for gene transfer

US were generated from a 0.5-inch diameter, IBMF-014 planar transducer with a center frequency of 1 MHz (Sofranel, Sartrouville, France). The transducer was placed in a custom made polystyrene tank filled with degassed pure water. A signal consisting of 1.0 MHz center frequency, 40% duty cycle and a pulse repetition frequency (PRF) of 10 kHz was generated by a 33220A arbitrary function generator (Agilent technologies, Les Ulis, France) and amplified by a RF power amplifier (ADECE, Artannes sur Indre, France) was used as the input for the transducer. Peak negative pressure of 150 kPa was used corresponding to an MI of 0.15. Ultrasound stimulation time was set to 60 seconds. The transducer was calibrated in a Perspex container using an HGL-200 PVDF bullet type hydrophone (Onda, Sunnyvale, CA) placed at 3 cm, the natural focal distance of the transducer and behind the first cuvette wall. Measures made with and without the cuvette wall conducted to an average of 5% attenuation. Reflections from the cuvette were measured in a separate experiment in our sonoporation setup. The transducer was driven using a 103 SPR pulser-receiver (Accu-Tron Inc). The reflections from the cuvette were measured to be lower than -13 dB, and could therefore be neglected. Furthermore, we investigated the influence of potential reflections from the 3-mm thick container wall using the same pulser-receiver. Here, we found, that reflections from the inner surface of the container were mostly cancelled out by the inverted-phase reflections from the outer surface of the container. The transducer was positioned in front of the

sonoporation cuvette as depicted in the figure 1 (Sarstedt AG & Co, Nümbrecht, Germany). 10^5 cells were grown on a resized Opticell® membrane (10×15 mm) (Nunc GmbH & Co. KG, Langenselbold, Germany). Opticell® membranes were transferred into polystyrene cuvettes (Sarstedt, Nümbrecht, Germany) containing 1.5 mL of OptiMEM medium (Invitrogen, Carlsbad, CA, USA) supplemented with 1% FCS. During sonoporation the cell medium was supplemented with 2.5 µg of pDNA and 5 µL of microbubbles and the cuvette was placed under gentle agitation using a magnetic stirrer. After sonoporation the membrane was placed in the incubator with the sonoporation medium on a 12-well cell culture plate.

Ultrasound exposure system for high-speed imaging

The behaviour of microbubbles during sonoporation was studied by high-speed imaging methods. We performed real-time visualization of sonoporation events to investigate how microbubbles behave towards cells as a function of the acoustic pressure. The different possibility of interactions between MicroMarker® microbubbles and cells was investigated using the optimal acoustic parameters (1 MHz, 40% DC, 10 kHz PRF), at 100, 150 and 200 kPa.

For fast camera imaging experiments, the transducer was placed in a custom-made aluminum sonication chamber with internal dimensions of 130×170×35 $(mm)^3$ was locked into to the *xy*-stage of a 200M inverted microscope (Carl Zeiss AG, Oberkochen, Germany) coupled with a LSM Axiovert 510 confocal scanning device (Carl Zeiss), using an EC Plan-Neofluar 40× magnification and 1.30 numerical aperture oil objective (DIC M27, Carl Zeiss AG), with automated z-stack functionality as shown in the figure 2. The color charge coupled device (CCD) of a Photron FastCam MC-2.1 high-speed camera (VKT Video Kommunikation GmbH, Pfullingen, Germany) was connected to the microscope. The sensor was rotated to make sure

that in all recorded movies, the ultrasound is directed from the bottom right to the top left of the frame. The peak-negative acoustic pressures were measured in the insonation tank at the objective's field of view and corresponded to a mechanical index (MI) of 0.1, 0.15 or 0.2. The day before experiment, 1.6×10^6 cells were seeded in an Opticell® chamber. Ultrasound contrast agents were injected into the cell culture chamber before each experiment.

Ultrasound contrast agent

In this study, Micromarker® (VisualSonics, La Frette S/seine, France) microbubbles were used. Micromarker® contrast agents contain a perfluorobutane (C_4F_{10}) gas encapsulated by a phospholipid shell and have a median diameter between 2.3 to 2.9 µm. Microbubbles were prepared according to manufacturer's protocol, Micromarker® suspension contained approximately 2×10^9 MB/mL.

Gene transfer efficacy

We determined the optimal acoustic parameters that give the maximal gene transfer on adherent HeLa cells using our set-up described in Figure 1. Four parameters were tested: the sound pressure (kPa), the time of ultrasound exposure (sec), the duty cycle (%) and the microbubble concentration (%). We tested different values of acoustic pressure (from 100 to 200 kPa), duty cycles from 10 to 60% and ultrasound exposure times ranging from 10 to 300 seconds. The importance of the amount of microbubbles was also evaluated. When a parameter was tested, the other parameters were fixed as follows: 150 kPa, 60 sec, 40% DC, 5 µL microbubbles.

The efficacy of sonoporation to deliver luciferase gene was determined by measuring the luciferase activity 24 h after sonoporation of HeLa cells in the presence of a plasmid encoding the luciferase reporter gene. Cells were harvested, lysed and the

luciferase activity was measured using a luminometer (Lumat LB9507, Berthold, Wildbach, Germany) after adding 100 µL of luciferase substrate (1 mM luciferin containing ATP) to 60 µL of cell lysate. The values were expressed as RLU (Relative Luciferase Unit), this level was reported to the protein concentration in RLU/mg prot. The protein concentration was measured by the bicinchoninic acid assay.

The gene transfer efficacy was also evaluated by flow cytometry when a plasmid encoding for the GFP reporter gene was used (pMAX, Lonza). 24 h after sonoporation cells were harvested, pelleted and re-suspended in PBS before flow cytometry analysis; 10000 cells were analyzed for each condition.

Cell viability assay

The cell viability was determined 24 h after sonoporation using the MTT colorimetric assay. Cells were incubated during 4 h at 37°C, 5% CO_2 in presence of 3-(4,5-dimethylthiazol-2-yl)-2,5-diphenyltetrazolium bromide (Sigma-Aldrich, St. Louis, USA) at 500 µg/mL. Cells were washed and incubated in a lysis buffer consisting of acidified isopropanol containing 3% of SDS (Sigma-Aldrich) allowing the solubilization of tetrazolium salts. Quantification was made measuring the optic density at 560 nm; the control optical density was made using cells having received the same manipulations without any treatment.

Microbubble fluorescent labelling

To probe MicroMarker® microbubbles, their envelope was stained with the fluorescent lipophilic probe DiD (λ_{ex} = 633 nm, λ_{em} = 643-670 nm) (Vybrant™, Molecular Probes®, Invitrogen, San Diego, CA, USA). A ratio of 1 µL of DiD to 40 µL MicroMarker® was used. The solution was homogenized by pipetting and it was used after 5 min incubation at room temperature.

Lipid raft labelling

To get more insight on interactions between microbubbles and cells, we identified if the region where microbubbles clustered on the cell surface could be some specific area of the plasma membrane as lipid rafts. Microbubbles were labelled with DiD lipophilic dye and lipid rafts were stained with Rhodamine B-tagged cholera toxin B-subunit (CTB, Molecular Probes, λ_{ex} = 543 nm, λ_{em} = 553-600 nm) known to interact with GM1 gangliosides, one constituent of lipid rafts (Antes *et al.*, 1992). HeLa cells were incubated with 2.5 µg/mL of CTB during 30 minutes at 37°C before sonoporation. Immediately after sonoporation cells were fixed using a 2% paraformaldehyde solution in PBS. After three washes, resized Opticell® membranes were then mounted on glass slides for confocal microscopy observations. Images were analyzed for colocalization by the plugin JACoP in ImageJ (Bolte and Cordelieres, 2006).

Importance of endocytosis during sonoporation

To assess if endocytosis is needed to get an efficient gene transfer following sonoporation a first experiment was the evaluation of incubation time of cells and plasmid DNA on gene transfer efficacy. Cells were sonoporated and the medium was retrieved and renewed with fresh medium immediately (0 h) or at different times up to 4 hours. Cells were harvested 24 hours later and the luciferase expression was measured as previously described.

To validate the involvement of endocytosis in the process of gene transfer by sonoporation, we tested the effect of depletion of cellular ATP and inhibitors of clathrin and caveolae-mediated endocytosis pathways on the sonoporation gene transfer efficacy. Cells were ATP-depleted by 30 minutes incubation in presence of

ATP depletion buffer (50 mM 2-deoxy-ATP, 50 mM sodium azide, 1.8 mM $CaCl_2$ in PBS pH 7.4) before the sonoporation. Cells were pre-treated for 30 minutes with either chlorpromazine (2.5 to 20 µg/mL; Sigma-Aldrich) an inhibitor of clathrin-mediated endocytosis pathway, Filipin III (1 to 4 µg/mL; Sigma-Aldrich) or Genistein (1 to 10 µg/mL), both inhibitors of caveolin-mediated endocytosis pathway (Ivanov, 2008). Then, sonoporation was performed in presence of indicated inhibitor and the cell medium was only replaced two hours later to maintain the inhibition effect.

Plasmid DNA internalization assay

The pDNA uptake by cells was evaluated by flow cytometry using a FITC-labelled plasmid. Trypan blue was used as a quencher of the FITC-fluorescence at the plasma membrane to distinguish pDNA attached to the plasma from internalized pDNA (Van Amersfoort and Van Strijp, 1994). Cells were harvested immediately (0), 3 or 6 hours after sonoporation and analyzed by flow cytometry (LSR, BD). 10 000 events were used for each condition.

Statistical analysis

Data was expressed as mean ± SD. Statistical differences between groups was analyzed by the bilateral Mann**–**Whitney U-test and the correlation analyses were conducted using the Spearman test using XLStat 2014 software (Addinsoft, Paris, France). The significance was defined as a *p*-value ≤ 0.05.

Results

Optimal acoustic parameters determination for efficient gene transfer.

Figure 3A shows the effect of the acoustic pressure on the gene transfer efficacy. Increasing the acoustic pressure from 100 to 160 kPa caused a linear improvement of the gene transfer efficacy (from 3.2×10^4 to 2×10^6 RLU/mg prot, 62-fold increase). The maximum level of gene expression was obtained at 160 kPa and it decreased with further increase in acoustic pressure. At 200 kPa, the efficacy was 10-fold lower than the level obtained at 160 kPa (1.9×10^5 RLU/mg prot). In our study, the cell viability was preserved (90% of cell viability) under the optimal condition for gene transfer.

As observed in Figure 3B, the gene transfer efficacy was positively improved with ultrasound exposure time between 10 and 60 seconds (2.1×10^4 and 5.4×10^5 RLU/mg prot respectively). A plateau was observed between 60 and 300 seconds. However, it should be noted that a high variability was observed for long stimulation times. Indeed, we observed a cell toxicity ranging from 30 to 60% for the respective ultrasound stimulation time of 10 and 300 seconds.

Regarding the duty cycle (Figure 3C), a threshold value of 40% duty cycle was required for an efficient gene transfer. Between 10 and 30% duty cycle, a very low expression level of luciferase gene was obtained (around 10^4 RLU/mg prot). At 40% duty cycle, there was 75-fold increase of gene transfer efficacy as compared to 10% duty cycle. Then, a plateau was reached between 40 and 60% duty cycle. However, experiments conducted at 60% duty cycle led to a low viability (40%).

Figure 3D shows that a minimum volume of microbubble of 2.5 µL is required to get an increased gene expression compared to control without microbubbles (6.2×10^5

RLU/ mg prot using 2.5 µL of microbubbles vs. 5.8×10^4 RLU/ mg prot for the control without microbubbles). No significant improvement was achieved when higher volumes were injected.

Microbubble behavior during sonoporation

Depending on the acoustic pressure used three different types of microbubble-cell interactions were observed (figure 4 and supplementary video). At 100 kPa, a cellular massage was the main observed phenomenon. Ultrasound-activated microbubbles remained in contact with the cell membrane during the whole stimulation (Figure 4A). At this acoustic pressure, a low level of gene transfer was obtained as seen on Figure 3A. At 150 kPa, an additional phenomenon consisting of the microbubble entry into cells was depicted (figure 4B). The microbubble was first interacting with cells and then disappeared after few milliseconds. In the presented sequence, two microbubbles (indicated by arrow heads) penetrated inside cells after 600 ms of ultrasonic stimulation. This observation is in accordance with our previous study (Delalande *et al.*, 2011). Note that the optimal gene transfer efficacy was obtained at this acoustic pressure range (Figure 3A). For a sound pressure of 200 kPa, microbubbles were either driven out from the field of view due to excessive radiation force or interacted violently with the cell. The latter induced the cell detachment from the support. At 200 kPa, the gene transfer efficacy was ten times lower than at 150 kPa that is likely due to the above-described phenomena.

Our real-time sonoporation result indicate that three event types could be recorded: microbubbles stuck on cell membrane during the insonation corresponding to the cellular massage; microbubbles entering into cells (translation) and microbubbles having a violent interaction with cells. Table 1 summarizes the correlation between

gene transfer efficacy and the different types of events recorded during sonoporation and the acoustic pressure used. A positive correlation could be measured between the gene transfer efficiency and the microbubble entry to cells ($p<0.0001$). Moreover the incidence of violent interactions was found positively correlated with the acoustic pressure ($p<0.0001$).

Lipids rafts and microbubble-cell interactions.

At optimal parameters for gene transfer, microbubbles were found mainly colocalized with lipid rafts immediately after sonoporation with a coefficient of colocalization of 0.706 and an overlapping coefficient of 0.803. This is shown by the purple color corresponding to a colocalization of DiD-labelled microbubbles presented in blue and Rhodamine B-labelled cholera toxin B presented in red (figure 5).

Plasmid DNA and microbubble intracellular routing upon sonoporation

Figure 6 presents the localization of plasmid DNA (red) in HeLa cells expressing Rab7-eGFP (green). Immediately after sonoporation, pDNA was mainly localized at the plasma membrane without any co-localization with Rab7-eGFP (Figures 6A and 6B). Observations from 3 hours post-sonoporation indicated that some of pDNA ended up into late endosomes as demonstrated by the yellow color (merge of green and red spots) revealing their localization in Rab7-positive organelles (Figures 6C and 6D).

Figure 7 presents the localization of plasmid DNA (red) and DiD-labelled microbubbles (blue) in HeLa cells expressing Nup153-eGFP (green). 6 hours post-sonoporation plasmid DNA was found to be close to the nuclear envelope, very few copies of plasmid DNA were observed in the nucleus. Microbubbles could also be observed in the cells after at this time point.

Figure 8 presents the kinetics of a FITC-labelled pDNA uptake after sonoporation by flow cytometry. When analyzing the cells immediately after sonoporation, 4% of cells were found positive for FITC fluorescence. The maximum of cells carrying sonoporated pDNA is reached (12.5%) upon 3 hours post-sonoporation. This value drops to 9.6% when trypan blue was added to quench the extracellular fluorescence meaning that most of pDNA was internalized at this time. After 6 hours post-sonoporation the percentage of cells carrying pDNA decreased to 3.5%. The mean fluorescence intensity values (MFI) obtained in different conditions without trypan blue treatment followed the same trend as the percentage of fluorescent cells. After 6 hours, a decrease of MFI value by 1.5 fold times was observed.

Endocytosis process involvement during sonoporation

Figure 9 shows the influence of time incubation on gene transfer efficacy. No significant gene transfer efficacy increase was found during the first hour of incubation. However, it was improved 15-times greater when the medium was removed upon 2 hours after sonoporation compared to an immediate washing. When the sonoporation medium was replaced after 4 hours post-sonoporation, it resulted in the highest gene transfer efficacy (1.82×10^8 RLU/mg prot), 328 times higher than when the medium was changed immediately following sonoporation process.

A sonoporation in an ATP-depletion condition conducted to a gene transfer efficacy 28-fold lower than the control (figure 10A). The use of caveolae pathway inhibitors Filipin III or Genistein had no significant effect on gene transfer by sonoporation (figures 10B and 10C). By contrast, there was a significant and dose-dependent inhibition when the clathrin-dependent endocytosis inhibitor used was chlorpromazine. The gene transfer was significantly decreased by 3, 5 and 140-fold

when cells were respectively incubated in presence of 7.5, 10 and 20 µg/mL chlorpromazine (figure 10D) corresponding to a decrease of 70, 82 and 99% of the luciferase expression obtained in control cells (p-value<0.05). No significant inhibition was observed with chlorpromazine concentration of 5 µg/mL. It is worth to note that a significant toxicity of chlorpromazine was obtained using a concentration of 20 µg/mL (approximately 30% of cell viability).

We validated the effectiveness of the endocytosis inhibition protocol by testing the effect on the internalization of transferrin, a positive control of the clathrin-dependent endocytosis pathway (data not shown). These conditions led also to an inhibition of transferrin uptake whilst little effect was obtained with cells incubated in the presence of Filipin III.

Discussion

The aim of this study was to investigate cellular events that occur during sonoporation from microbubble-cell interactions, intracellular plasmid DNA routing and transgene expression.

Optimal parameters determination

The levels of luciferase activity obtained were in the same range as those reported in our previous results obtained with HeLa cells in suspension in the presence of BR14 microbubbles (Kaddur *et al.*, 2010). In this study, a plateau was also reached at 40% duty cycle.

Duvshani *et al.* obtained also similar results when they performed sonoporation on mouse prostate adenocarcinoma cells although their experiments have been conducted with Optison™ (Duvshani-Eshet and Machluf, 2007). The ultrasound settings used in this study were similar in acoustic pressure, duty cycle and

frequency but not for the insonation time that was between 10 to 30 minutes. In another study performed on HeLa cells using SonoVue®, Li *et al.* have found that a maximum efficacy was obtained for an ultrasonic stimulation of 240 kPa for 7 minutes with a duty cycle of 60%. However, they measured a high toxicity (30% of cell viability) (Li *et al.*, 2009). The high variability that we observed after increasing stimulation time could be explained by an increase in the toxicity induced by sonoporation with time of stimulation. A minimum volume of microbubbles was necessary to reach a good gene transfer efficacy. The microbubble concentration used was similar to that previously obtained on HeLa cells in suspension in the presence of microbubbles BR14 (Kaddur *et al.*, 2010) and the study of Rahim *et al.* performed on CHO cells adherent in the presence of SonoVue® (Rahim *et al.*, 2006). The gene transfer efficacy was often decreased when too many microbubbles (above 10 µL) were in the presence of cells due to the formation of microbubble clusters reducing microbubble-cell interactions or either to the cell toxicity as observed previously (Nomikou *et al.*, 2012).

Taken together, the results obtained from the optimal acoustic parameters determination reflect the importance of each parameter used in ultrasound effectiveness for gene transfer mediated by sonoporation.

Microbubble-cell interactions

Depending on the settings used, the microbubble-cell interactions could be changed. Therefore, we established a sonoporation device coupled to a high-speed camera to observe these interactions in real time. The high speed imaging results showed that during ultrasound stimulation (1 MHz, 150 kPa, 40% duty cycle), microbubbles were interacting with cell membranes as observed in our previous studies (Delalande *et al.*, 2013; Delalande *et al.*, 2011). At this precise acoustic setting the microbubble entry in

cells was preferentially observed and this parameter gave the highest gene transfer. A positive correlation between these two events could mean that the entry of the microbubble while entering directly or indirectly promotes the pDNA delivery into the cell. The microbubble entrance could allow extracellular calcium entry (Fan *et al.*, 2012) and this calcium could trigger endocytosis (MacDonald *et al.*, 2005).

As we could expect microbubbles do not interact with random areas of the cell. The preferential localization of microbubbles during sonoporation is in lipid raft region. Because oscillating microbubbles are attracted to each other this localization might be explained by the fact that microbubbles are attracted to acoustically active areas in the cell. At this location, plasma membrane is composed of cluster of lipids enriched with cholesterol and sphingomyelin occupying at least 50% of the plasma the membrane (Jurak *et al.*, 2014). These areas are dynamic membrane domains tightly packed by lipid-lipid interactions. Moreover, cholesterol and sphingolipids are known to rigidify the plasma membrane; thus microbubbles could be attracted to these rigid parts of the plasma membrane. Note that lipid raft area has been reported to be active in terms of endocytosis process (Ares and Ortiz, 2012). This hypothesis is in line with the sonophore formation in the plasma membrane described by Krasovitski *et al.* (Krasovitski *et al.*, 2011). Sonophores are the expansion of a gap between the two membranes leaflets due to cavitation during the ultrasound negative peak pressure; this expansion stretches the plasma membrane until rupture to create a pore. Sonophores could be mainly formed either in the vicinity or in lipid raft areas and therefore attract microbubbles to this location. Microbubbles could be attracted to these areas because oscillating sonophores act like oscillating microbubble, due to the clustering phenomenon because in-phase oscillating objects are clustering (Kotopoulis and Postema, 2010). Moreover oscillating microbubble interacts

differently when in contact to a surface for example microbubbles will collapse asymmetrically next to rigid surface (Prentice *et al.*, 2005). We could imagine that the cell surface rigidity mismatch between lipid raft areas and the rest of the cell could create a preferential interaction site with microbubbles.

Plasmid DNA cellular routing after sonoporation

A key to success of this delivery method lies in understanding not only the mechanism governing microbubble and cell interactions but also the fate of pDNA after sonoporation. The internalization process of the plasmid DNA after sonoporation was found to be a slow phenomenon. 4 hours of interaction time between plasmid DNA and the cells was needed to get the maximum of gene transfer efficacy and flow cytometry analyses showed that the plasmid DNA was mainly internalized after 3 hours. Real-time confocal microscopy investigations showed that pDNA was mainly localized at the plasma membrane straightaway following sonoporation and these spots could progressively move inside cells as we have observed previously (Delalande *et al.*, 2013). These structures could correspond either to vesicles (endosome) or aggregates-like structures upon sonoporation. The presence of free pDNA not co-localized with Rab7-eGFP vesicles observed in figures 6A and 6C indicates that some of them might be able to escape the lysosome pathway or they could also be the result of a direct entrance across the plasma membrane during the sonoporation. The presence of microbubbles and pDNA inside cells raises the question about their cellular entry pathway. The kinetics of pDNA uptake shows that only the combination of ultrasound and microbubbles was able to efficiently drive pDNA inside the cells.

Our observations indicated also that pDNA were not observed into the nucleus, spots were close to the nucleus as indicated by their localization in the vicinity of nuclear

envelope delimited by Nup153-eGFP. However, we found in the same conditions a good gene transfer efficiency meaning that pDNA reach the nucleus this discrepancy could be due to a weaker fluorescent signal when the plasmid DNA reaches the nucleus (Maury *et al.*, 2014). The amount of pDNA found close to or inside the nucleus was not abundant compared to the pDNA entered into the cell observed at earlier time points suggesting a massive degradation or efflux of pDNA as observed after 6 hours by the decrease of MFI value by 1.5 fold times. However, this decrease was not as much as the one observed for the cell percentage which dropped from 9.6 at 3 hours to 3.5% at 6 hours. This reveals that some cells, likely those that had internalized a low amount of pDNA, have lost completely their content as indicated by the reduction of the cell percentage. The sonoporation efficacy could be improved at this step. In our study, the routing of the pDNA to the nucleus was also facilitated by the presence of optimal NFκB binding consensus sequence put upstream of the CMV promoter of the luciferase coding sequence (Goncalves *et al.*, 2009).

The maximum of cells carrying sonoporated pDNA is reached (12.5%) upon 3 hours post-sonoporation as a consequence of internalization process. When considering the values obtained after trypan blue treatment, the increase of MFI value after 3 hours was not as much as that observed with the percentage of cells. This observation suggests that during 3 hours after sonoporation, a new cell population took up pDNA via endocytosis process as validated by the increase of FITC-positive cell percentage. However, the amount of pDNA internalized during 3 hours was not very much higher than that occurred during the sonoporation process as indicated by the very slight increase of MFI value. This is in agreement with the fact that free pDNA were hardly up taken by cells and that microbubbles could not bind to pDNA to improve its internalization.

Involvement of endocytosis during sonoporation process

The impact of endocytosis on the sonoporation efficacy was shown in two ways.

After 6 hours the quantity of cells carrying plasmid DNA drops to 3.5% probably because of the degradation of the internalized pDNA. Free pDNA lifetime in cytosol has been estimated to be between 50 and 90 min (Lechardeur *et al.*, 1999). A part of pDNA endocytosed in Rab7 vesicles, as observed in figure 6C, may also reach the lysosome pathway to be degraded (Bucci *et al.*, 2000).

The use of endocytosis inhibitors showed that the main endocytosis pathway routing plasmid DNA was the clathrin-dependent pathway. The lack of significant gene transfer inhibition using caveolae inhibitors was unexpected because of the preferential localization of microbubbles observed in the lipid raft area. A correlation between this localization and caveolae endocytosis would have been expected (Lajoie and Nabi, 2010). The results obtained with chlorpromazine are in the same line as those obtained by Meijering *et al.*; they have reported that a 50% inhibition of 500-kDa dextran delivery by sonoporation was obtained when endothelial cells were treated with chlorpromazine (Meijering *et al.*, 2009). In contrast to our results, these authors have observed an inhibition with the Filipin III, this difference could be due to the size of the molecule transferred that was smaller (500 kDa for the dextran *versus* 3 MDa for the plasmid) and/or to the difference in cell type used. The reason why clathrin-dependent endocytosis pathway is more effective to deliver plasmid DNA rather than the caveolae pathway remains unknown. For example, the endocytosis route of lipoplexes or polyplexes can be different in function of their chemical composition (Billiet *et al.*, 2012).

The main limitation of this study lies in the fact that all the experiments have been done in separate experiments. A single-cell study of the sonoporation process would be the best to prove the correlation between all the phenomena observed.

Conclusion

We have found the optimal ultrasound parameters in our set-up for an efficient gene delivery on HeLa adherent cells. This study showed the cell-microbubbles interactions and the intracellular fate of microbubbles and pDNA during and after the sonoporation process. A set-up combining high speed camera coupled with confocal fluorescence microscopy has allowed us to observe that depending on the acoustic pressure used, some microbubble were forced to enter the cell during sonoporation whilst other were stuck at the plasma membrane. The microbubbles were found to enter in cells only in the best conditions of transfection suggesting that the microbubble entry could be closely correlated to the pDNA entry into the cell. By combining fluorescent pDNA with cellular tools exhibiting fluorescent intracellular compartments, confocal microscopy observations and uptake experiments indicated that the pDNA were taken up by cells through clathrin-mediated-endocytosis pathway as confirmed by their localization inside late endosomes and the effect of the pharmacological inhibitors. It is worth noting that the observations made in this study may not be translated to other nucleic acids and particularly for small molecules oligonucleotides as siRNA. Knowing this intracellular fate of microbubble and pDNA will be helpful for a rational design of potent sonoporation for gene delivery that might be combined with molecular imaging.

518 **Acknowledgements**

519 The authors thank the French “Région Centre” and National Research Agency for
520 funding.

References

Afadzi M, Strand SP, Nilssen EA, Masoy SE, Johansen TF, Hansen R, Angelsen BA, Davies CD. Mechanisms of the Ultrasound-Mediated Intracellular Delivery of Liposomes and Dextrans. IEEE Trans. Ultrason. Ferroelectr. Freq. Control 2013;60:21-33.

Antes P, Schwarzmann G, Sandhoff K. Detection of protein mediated glycosphingolipid clustering by the use of resonance energy transfer between fluorescent labelled lipids. A method established by applying the system ganglioside GM1 and cholera toxin B subunit. Chem Phys Lipids 1992;62:269-80.

Ares GR, Ortiz PA. Dynamin2, Clathrin, and Lipid Rafts Mediate Endocytosis of the Apical Na/K/2Cl Cotransporter NKCC2 in Thick Ascending Limbs. J. Biol. Chem. 2012;287:11.

Bao S, Thrall BD, Miller DL. Transfection of a reporter plasmid into cultured cells by sonoporation in vitro. Ultrasound Med Biol 1997;23:953-9.

Billiet L, Gomez JP, Berchel M, Jaffres PA, Le Gall T, Montier T, Bertrand E, Cheradame H, Guegan P, Mevel M, Pitard B, Benvegnu T, Lehn P, Pichon C, Midoux P. Gene transfer by chemical vectors, and endocytosis routes of polyplexes, lipoplexes and lipopolyplexes in a myoblast cell line. Biomaterials 2012;33:2980-90.

Bolte S, Cordelieres FP. A guided tour into subcellular colocalization analysis in light microscopy. Journal of microscopy 2006;224:213-32.

Bucci C, Thomsen P, Nicoziani P, McCarthy J, van Deurs B. Rab7: a key to lysosome biogenesis. Mol Biol Cell 2000;11:467-80.

Delalande A, Bouakaz A, Renault G, Tabareau F, Kotopoulis S, Midoux P, Arbeille B, Uzbekov R, Chakravarti S, Postema M, Pichon C. Ultrasound and microbubble-assisted gene delivery in Achilles tendons: Long lasting gene expression and restoration of fibromodulin KO phenotype. J Control Release 2011;156:223-30.

Delalande A, Kotopoulis S, Postema M, Midoux P, Pichon C. Sonoporation: Mechanistic insights and ongoing challenges for gene transfer. Gene 2013;525:191-9.

Delalande A, Kotopoulis S, Rovers T, Pichon C, Postema M. Sonoporation at a low mechanical index. Bubble science, Engineering and Technology 2011;3:3-11.

Delalande A, Postema M, Mignet N, Midoux P, Pichon C. Ultrasound and microbubble-assisted gene delivery: recent advances and ongoing challenges. Therapeutic Delivery 2012;3:1199-215.

Duvshani-Eshet M, Machluf M. Efficient transfection of tumors facilitated by long-term therapeutic ultrasound in combination with contrast agent: from in vitro to in vivo setting. Cancer gene therapy 2007;14:306-15.

Fan Z, Liu H, Mayer M, Deng CX. Spatiotemporally controlled single cell sonoporation. Proc Natl Acad Sci U S A 2012;109:16486-91.

Goncalves C, Ardourel MY, Decoville M, Breuzard G, Midoux P, Hartmann B, Pichon C. An optimized extended DNA kappa B site that enhances plasmid DNA nuclear import and gene expression. J Gene Med 2009;11:401-11.

Ivanov AI. Pharmacological inhibition of endocytic pathways: is it specific enough to be useful? Methods in molecular biology (Clifton, N.J 2008;440:15-33.

Juffermans LJ, Meijering DB, van Wamel A, Henning RH, Kooiman K, Emmer M, de Jong N, van Gilst WH, Musters R, Paulus WJ, van Rossum AC, Deelman LE, Kamp O. Ultrasound and microbubble-targeted delivery of therapeutic compounds: ICIN Report

Project 49: Drug and gene delivery through ultrasound and microbubbles. Neth Heart J 2009;17:82-6.

Jurak M, Golabek M, Holysz L, Chibowski E. Properties of Langmuir and solid supported lipid films with sphingomyelin. Advances in colloid and interface science 2014.

Kaddur K, Lebegue L, Tranquart F, Midoux P, Pichon C, Bouakaz A. Transient transmembrane release of green fluorescent proteins with sonoporation. IEEE Trans Ultrason Ferroelectr Freq Control 2010;57:1558-67.

Kotopoulis S, Postema M. Microfoam formation in a capillary. Ultrasonics 2010;50:260-8.

Krasovitski B, Frenkel V, Shoham S, Kimmel E. Intramembrane cavitation as a unifying mechanism for ultrasound-induced bioeffects. Proc Natl Acad Sci U S A 2011;108:3258-63.

Kurosaki T, Kawakami S, Higuchi Y, Suzuki R, Maruyama K, Sasaki H, Yamashita F, Hashida M. Development of anionic bubble lipopolyplexes for efficient and safe gene transfection with ultrasound exposure in mice. Journal of Controlled Release 2014;176:24-34.

Lajoie P, Nabi IR. (2010) LIPID RAFTS, CAVEOLAE, AND THEIR ENDOCYTOSIS, In: Jeon KW, ed. *International Review of Cell and Molecular Biology, Vol 282*. San Diego: Elsevier Academic Press Inc, 135-63.

Lechardeur D, Sohn KJ, Haardt M, Joshi PB, Monck M, Graham RW, Beatty B, Squire J, O'Brodovich H, Lukacs GL. Metabolic instability of plasmid DNA in the cytosol: a potential barrier to gene transfer. Gene Ther 1999;6:482-97.

Li YS, Davidson E, Reid CN, McHale AP. Optimising ultrasound-mediated gene transfer (sonoporation) in vitro and prolonged expression of a transgene in vivo: potential applications for gene therapy of cancer. Cancer Lett 2009;273:62-9.

MacDonald PE, Eliasson L, Rorsman P. Calcium increases endocytotic vesicle size and accelerates membrane fission in insulin-secreting INS-1 cells. J Cell Sci 2005;118:5911-20.

Maury B, Goncalves C, Tresset G, Zeghal M, Cheradame H, Guegan P, Pichon C, Midoux P. Influence of pDNA availability on transfection efficiency of polyplexes in non-proliferative cells. Biomaterials 2014;35:5977-85.

Mehier-Humbert S, Bettinger T, Yan F, Guy RH. Plasma membrane poration induced by ultrasound exposure: implication for drug delivery. J Control Release 2005;104:213-22.

Meijering BD, Juffermans LJ, van Wamel A, Henning RH, Zuhorn IS, Emmer M, Versteilen AM, Paulus WJ, van Gilst WH, Kooiman K, de Jong N, Musters RJ, Deelman LE, Kamp O. Ultrasound and microbubble-targeted delivery of macromolecules is regulated by induction of endocytosis and pore formation. Circ Res 2009;104:679-87.

Miller DL, Bao S, Morris JE. Sonoporation of cultured cells in the rotating tube exposure system. Ultrasound Med Biol 1999;25:143-9.

Noble ML, Kuhr CS, Graves SS, Loeb KR, Sun SS, Keilman GW, Morrison KP, Paun M, Storb RF, Miao CH. Ultrasound-targeted microbubble destruction-mediated gene delivery into canine livers. Mol Ther 2013;21:1687-94.

Nomikou N, Tiwari P, Trehan T, Gulati K, McHale AP. Studies on neutral, cationic and biotinylated cationic microbubbles in enhancing ultrasound-mediated gene delivery in vitro and in vivo. Acta Biomater 2012;8:1273-80.

611 Paula DM, Valero-Lapchik VB, Paredes-Gamero EJ, Han SW. Therapeutic ultrasound
612 promotes plasmid DNA uptake by clathrin-mediated endocytosis. J Gene Med
613 2011;13:392-401.

614 Pichon C, Kaddur K, Midoux P, Tranquart F, Bouakaz A. Recent advances in gene delivery
615 with ultrasound and microbubbles. J. Exp. Nanosci. 2008;3:17-40.

616 Postema M, Gilja OH. Ultrasound-directed drug delivery. Current pharmaceutical
617 biotechnology 2007;8:355-61.

618 Prentice P, Cuschierp A, Dholakia K, Prausnitz M, Campbell P. Membrane disruption by
619 optically controlled microbubble cavitation. Nat. Phys. 2005;1:107-10.

620 Rahim A, Taylor SL, Bush NL, ter Haar GR, Bamber JC, Porter CD. Physical parameters
621 affecting ultrasound/microbubble-mediated gene delivery efficiency in vitro.
622 Ultrasound Med Biol 2006;32:1269-79.

623 Taniyama Y, Tachibana K, Hiraoka K, Namba T, Yamasaki K, Hashiya N, Aoki M, Ogihara T,
624 Yasufumi K, Morishita R. Local delivery of plasmid DNA into rat carotid artery using
625 ultrasound. Circulation 2002;105:1233-9.

626 Van Amersfoort ES, Van Strijp JA. Evaluation of a flow cytometric fluorescence quenching
627 assay of phagocytosis of sensitized sheep erythrocytes by polymorphonuclear
628 leukocytes. Cytometry 1994;17:294-301.

629 Wang X, Liang HD, Dong B, Lu QL, Blomley MJ. Gene transfer with microbubble ultrasound
630 and plasmid DNA into skeletal muscle of mice: comparison between commercially
631 available microbubble contrast agents. Radiology 2005;237:224-9.

632 Zhou Y, Kumon RE, Cui J, Deng CX. The Size of Sonoporation Pores on the Cell Membrane.
633 Ultrasound Med Biol 2009.

634

Figure captions

Figure 1 - *In vitro* sonoporation set-up used for gene transfer experiments.

Figure 2 - *In vitro* set-up used for high-speed imaging experiments. The top panel represents an overview of the devices used; the bottom panel is a close-up view of the water tank mounted on the microscope.

Figure 3 - Optimal sonoporation parameters determination. (A) Influence of the acoustic pressure (parameters: 5 µL MB, 60 sec, 40% DC, 2.5 µg pDNA). (B) Influence of the time of insonation (parameters: 150 kPa, 5 µL MB, 40% DC, 2.5 µg pDNA). (C) Influence of the duty cycle (DC) (parameters: 150 kPa, 60 sec, 5 µL MB, 2.5 µg pDNA). (D) Influence of the concentration in microbubbles (parameters: 150 kPa, 60 sec, 40% DC, 2.5 µg pDNA). Values shown represent means of 3 experiments done in duplicates.

Figure 4 - Sequences of images of HeLa cells in the presence of microbubbles; (A) images taken during an ultrasound stimulation at 100 kPa, the microbubble surrounded interacts with the plasma membrane by cellular "massage"; (B) images taken during an ultrasound stimulation at 150 kPa, the arrowed microbubbles shrink before entering in the cell; (C) images taken during an ultrasound stimulation at 200 kPa, a microbubble interacts with a cell and detaches it from its support. The arrows show the microbubbles to observe over time. The time displayed corresponds to the value after the start of the ultrasound stimulation.

Figure 5 – Localization of MB to cell membrane interaction area after sonoporation by confocal microscopy. (A) Lipid raft areas were labelled by RhodB-cholera toxin subunit B (red) and MB were labelled with DiD (blue). (B) A high level of colocalization (purple) between MB and lipid rafts was found showing that during

ultrasound stimulation MB are preferentially interacting with cell membrane in lipid rafts areas. The white rectangle shows a magnified view of the plasma membrane used for the colocalization analysis (r=0.70).

Figure 6 - Localization of pDNA relative to late endosomes. HeLaRab7-eGFP cells were sonoporated at optimal acoustic parameters in presence of 2.5 µg of Cy3-tagged pDNA and microbubble. Green and red staining correspond to Rab7-eGFP positive late endosomes and pDNA-Cy3, respectively. Yellow color corresponds to a co-localization of pDNA and Rab7 (arrows). Confocal microscopy observations were made either immediately after sonoporation (A, B) or 3 hours post-sonoporation (C, D). A and C: phase contrast images; B and D: merge of green (Rab7-eGFP) and red (pDNA-Cy3) fluorescence images. White dotted lines in the right frames indicate the cell plasma membrane boundary and the arrows show colocalization spots between Rab7-GFP endosomes and pDNA-Cy3.

Figure 7 - Localization of pDNA relative to the nucleus 6 h post-sonoporation. HeLaNup153-eGFP cells were sonoporated at optimal acoustic parameters in presence of 2.5 µg of Cy3-tagged pDNA and DiD labelled microbubbles (blue). The green staining corresponds to Nup153-eGFP, which delimits the cell nucleus. Some plasmids were found close to the nucleus 6 hours after sonoporation. Microbubbles were still found in the cytoplasm and in the nucleus 6 hours after sonoporation. A: phase contrast image, B: merge of green (Nup153-eGFP), red (pDNA-Cy3) and blue (MB-DiD) fluorescence images.

Figure 8 – Analysis of plasmid DNA internalization after sonoporation. Cells were sonoporated using the optimal acoustic parameters with 2.5 µg of FITC labelled plasmid DNA. The presence of plasmid DNA on cells was analyzed by flow cytometry immediately (white), 3 (grey) and 6 (black) hours after sonoporation in presence or

not of trypan blue. Trypan blue was used to quench FITC fluorescence from plasma membrane; the remaining fluorescence corresponds to internalized plasmid DNA. The histograms represent the percentage of FITC-positive cells and the squares represent the mean fluorescence intensity (MFI) of the cells in each condition.

Figure 9 – Gene transfer efficacy by the function of sonoporation medium incubation time. The cell medium was replaced by fresh medium immediately (0), 0.5, 1, 2 or 4 hours after sonoporation. The gene transfer efficacy was evaluated 24 hours after sonoporation and expressed as RLU/mg prot. The values represent means and standard error of at least 3 experiments.

Figure 10 - Effect of cellular ATP depletion and endocytosis inhibitors on the efficacy of gene transfer by sonoporation (A: ATP depletion; B: Filipin III; C: Genistein; D: Chlorpromazine). Parameters used: 1 MHz, 60 sec, 150 kPa, 40% DC, 5 µL MB, 10 µg pDNA. The gene transfer efficacy and the cell viability were determined 24 hours after sonoporation. Values represent mean of luciferase activity in RLU/mg prot. *: statistical difference compared to control with a *p*-value < 0.05.

Supplementary video 1.

The video shows 3 sequences of images of HeLa cells in the presence of microbubbles; (1) images taken during an ultrasound stimulation at 100 kPa, the microbubble surrounded interacts with the plasma membrane by cellular "massage"; (2) images taken during an ultrasound stimulation at 150 kPa, the arrowed microbubbles shrink before entering in the cell; (3) images taken during an ultrasound stimulation at 200 kPa, a microbubble interacts with a cell and detaches it from its support.

708 **Table 1.**

Peak negative acoustic pressure (kPa)	Gene transfer efficacy (RLU/mg proteins)	Microbubble-cell interaction type observed			
		Microbubble stuck to cell membrane (%)	Microbubble entry to cell (%)	Violent microbubble-cell interactions (%)	Videos recorded (n)
100	3.2×10^{4}	86	14	0	9
150	1.8×10^{6}	39	43	18	45
200	1.9×10^{5}	33	24	53	21

709 Table 1. Comparison between gene transfer efficacy values and microbubble-cell interaction type observed by

710 high speed imaging.

Figure 1

Click here to download Figure: Figure 1.pdf

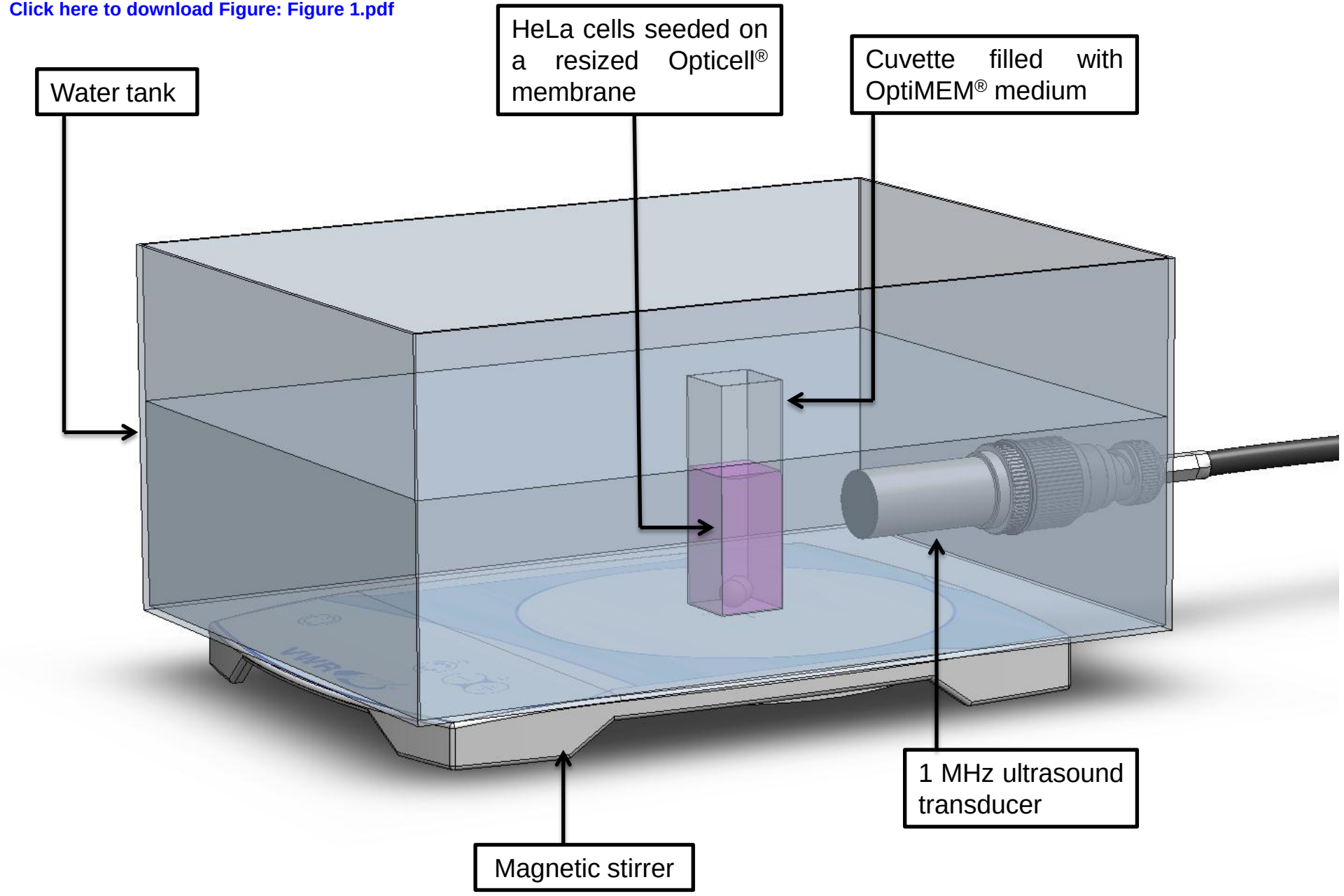

Figure 2

Click here to download high resolution image

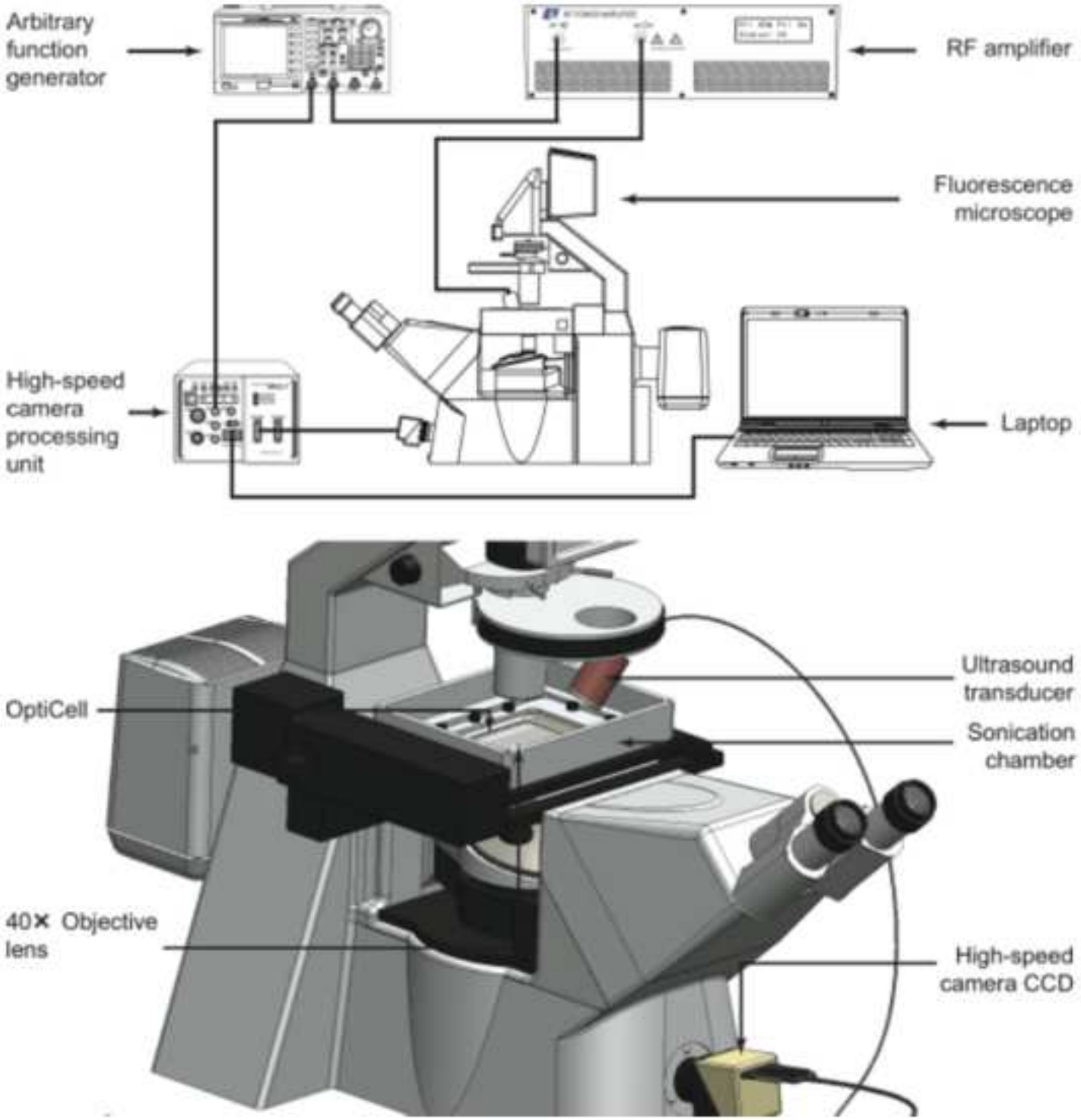

Figure 3

Click here to download Figure: Figure 3.pdf

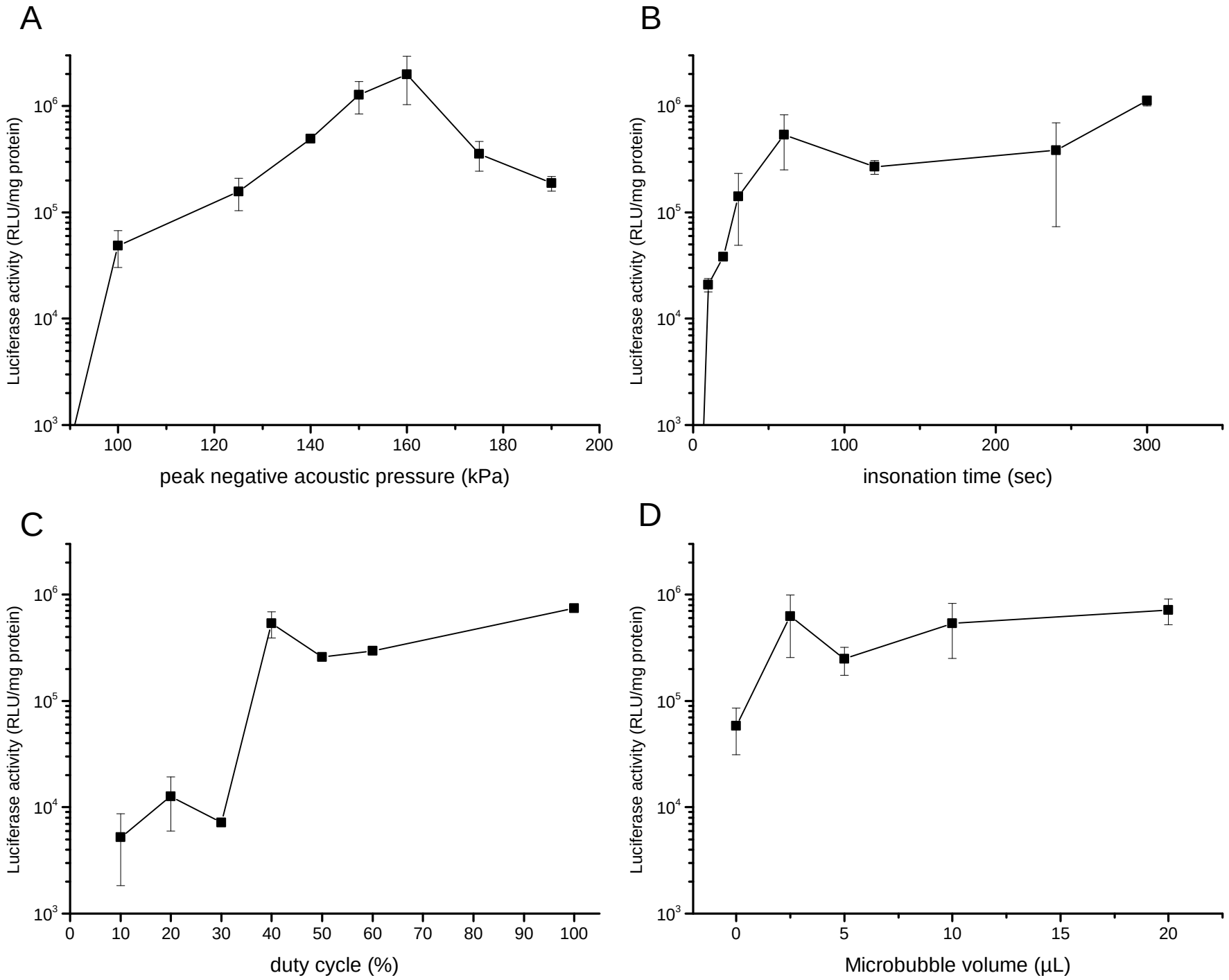

Figure 4
Click here to download Figure: Figure 4rev2.pdf

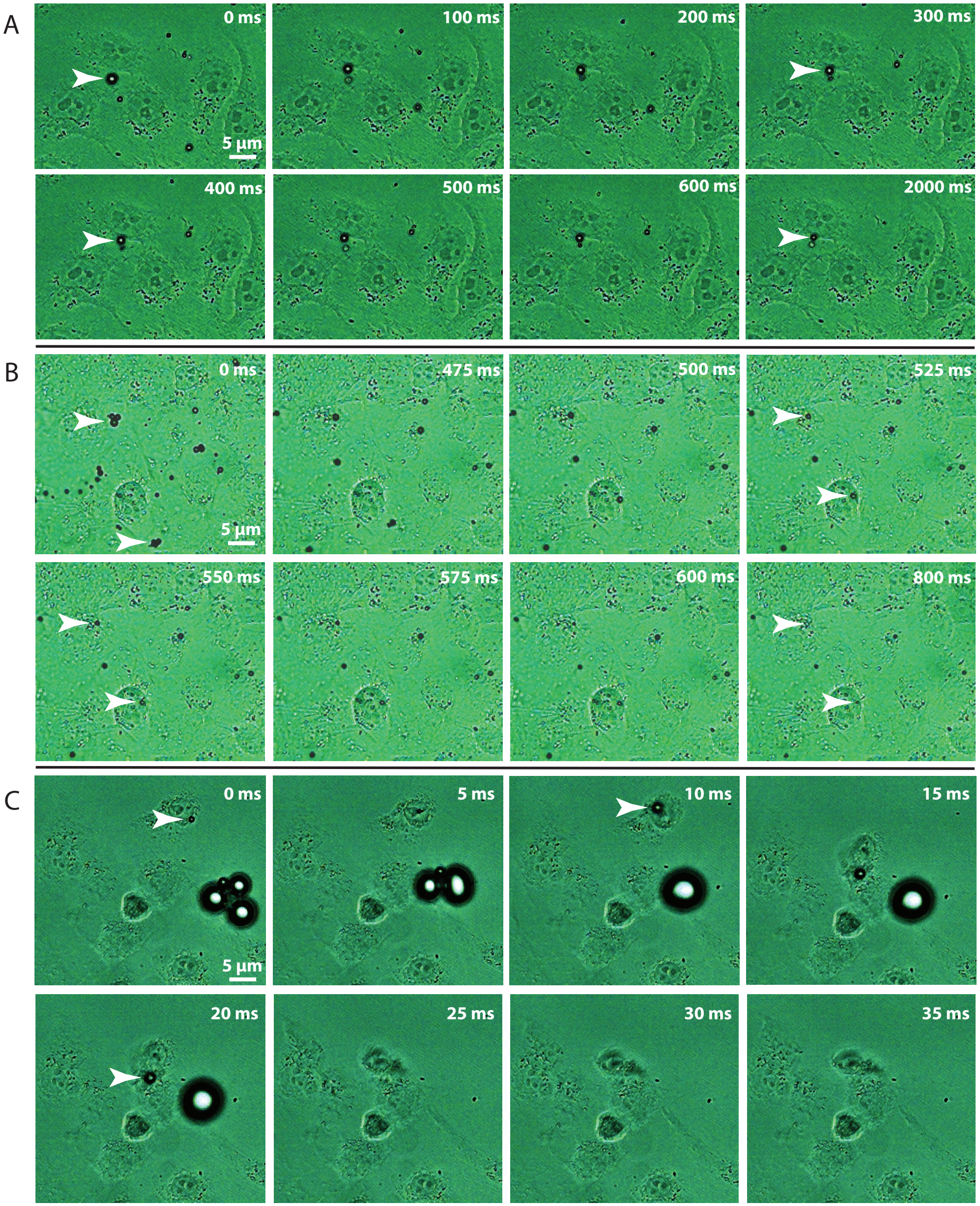

Figure 5

Click here to download Figure: Figure 5.pdf

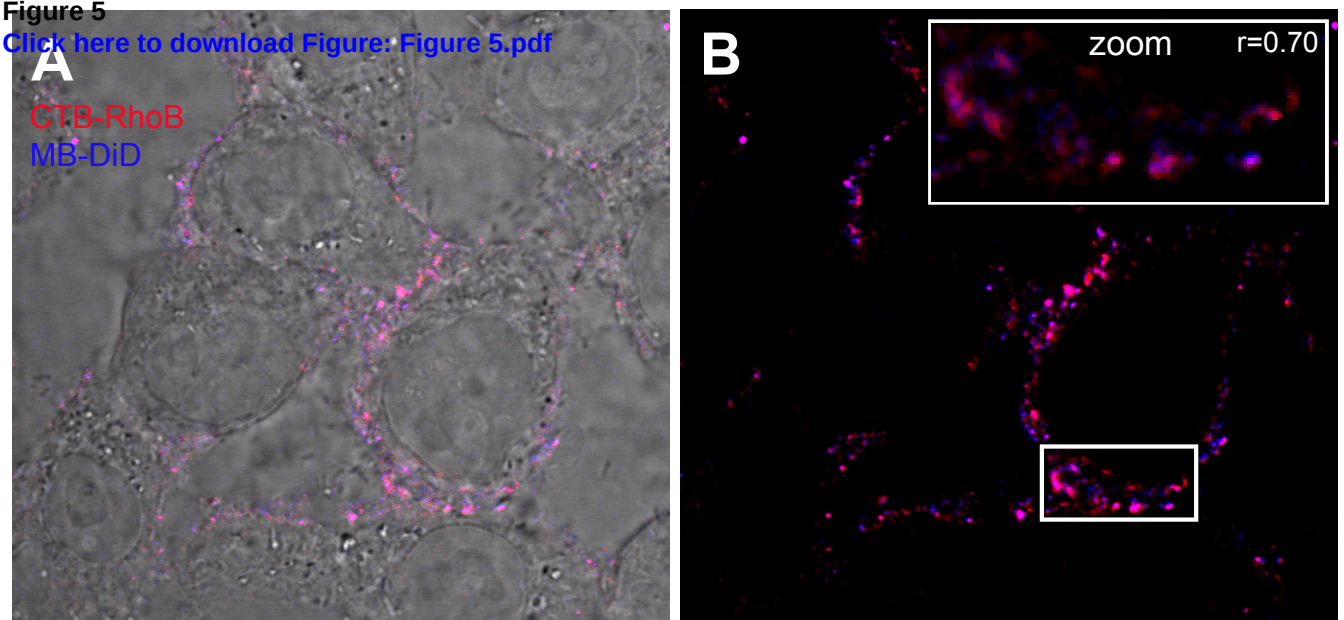

Figure 6

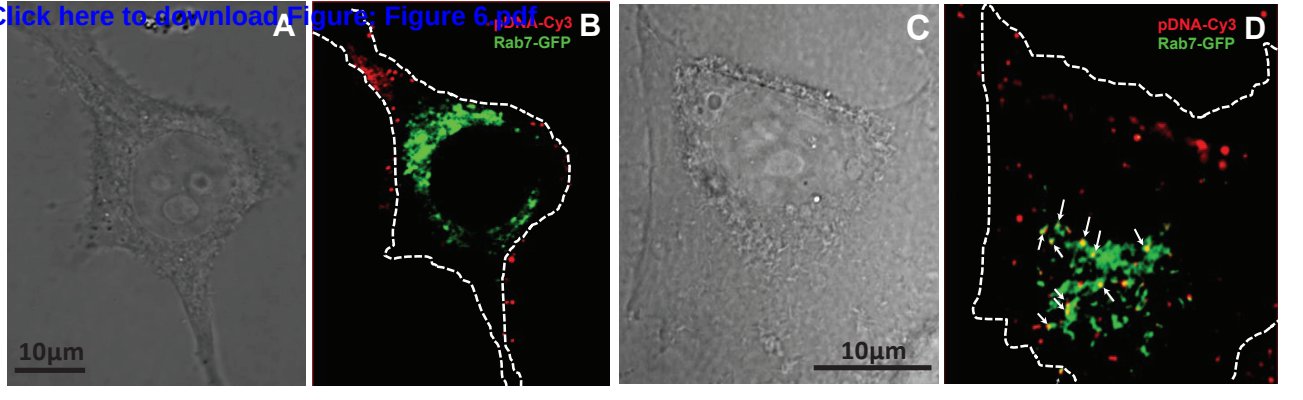

Figure 7

Click here to download Figure: Figure 7.pdf

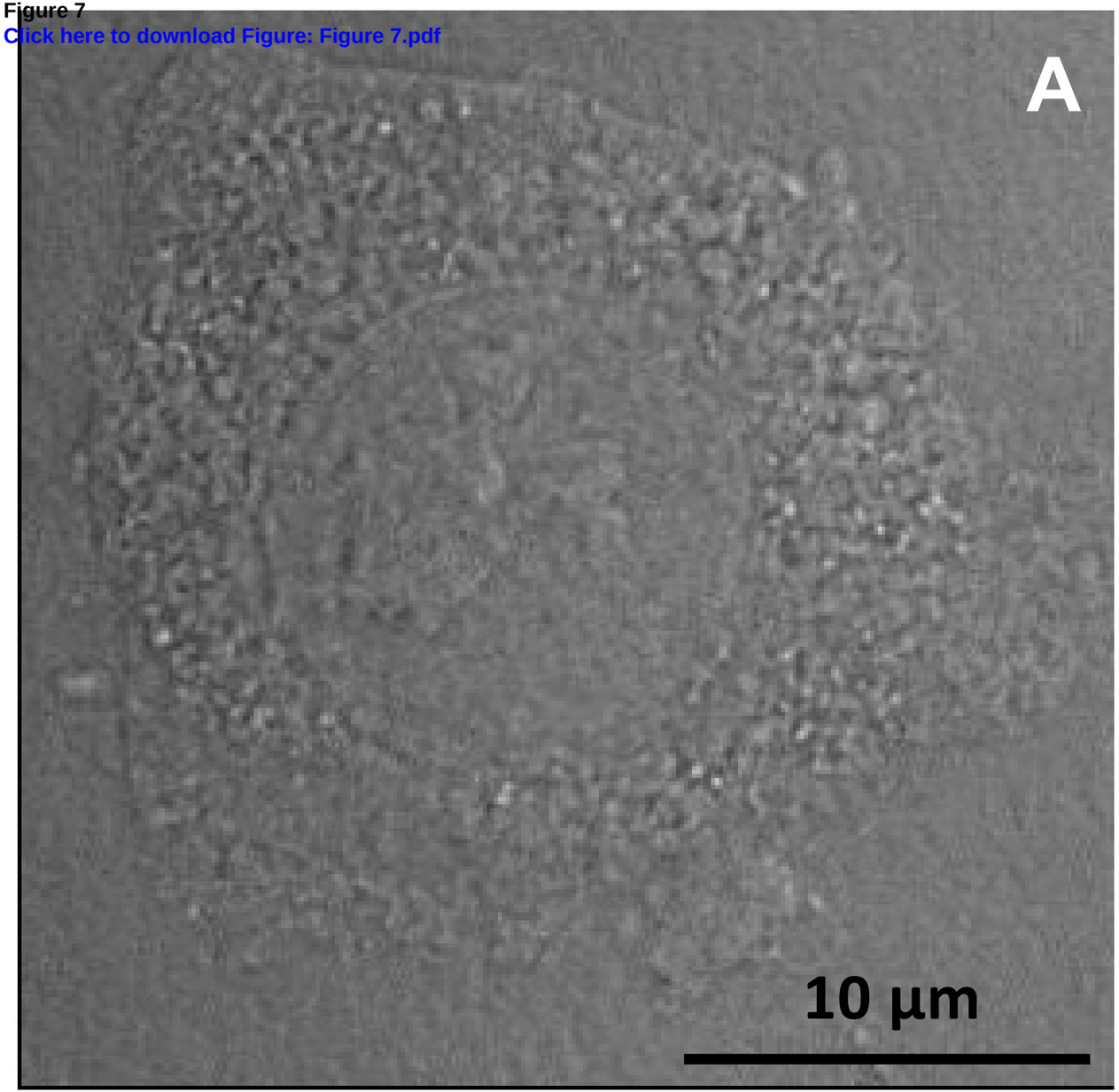

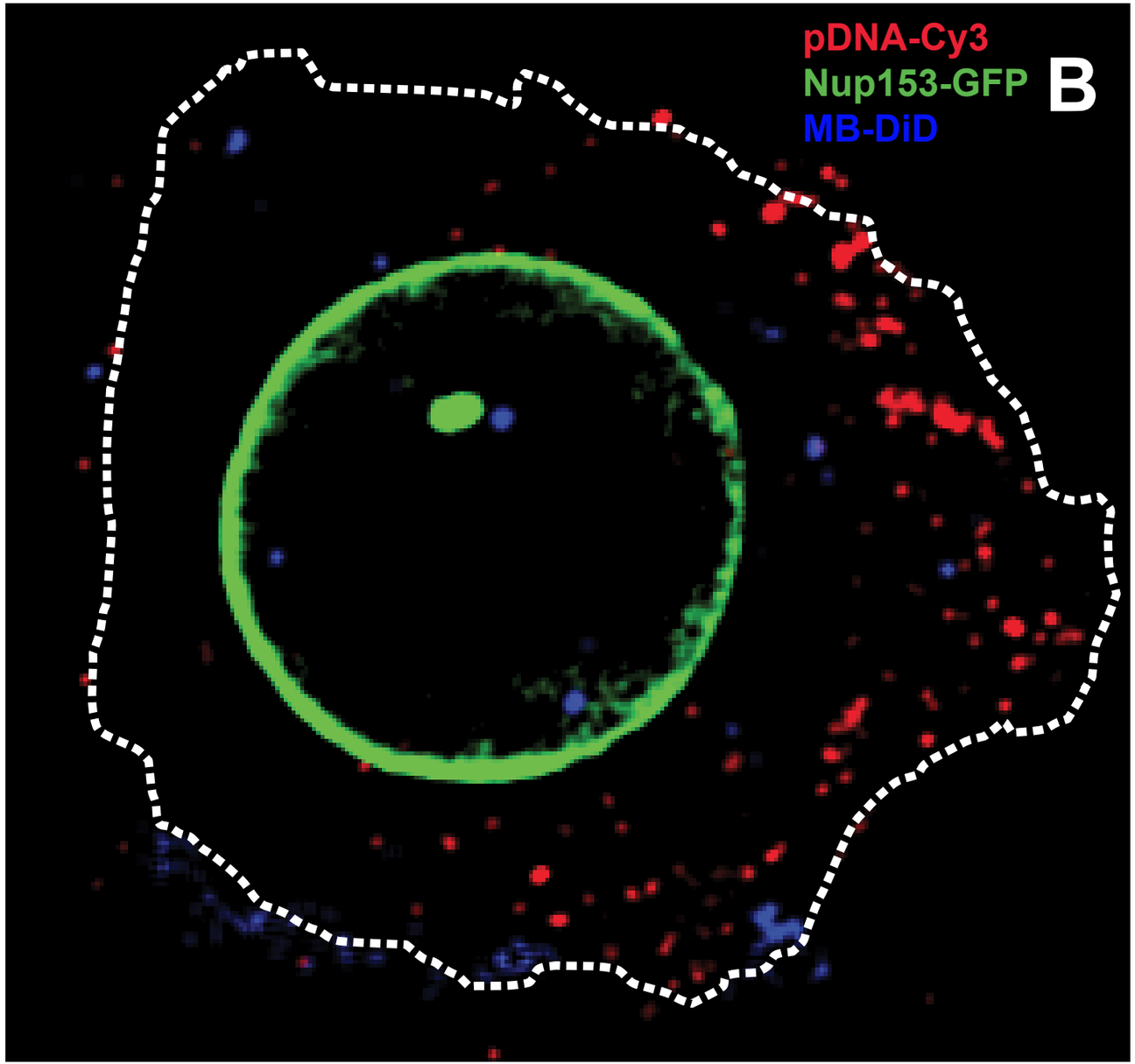

Figure 8

Click here to download Figure: Figure 8-06-06-14-19-40.pdf

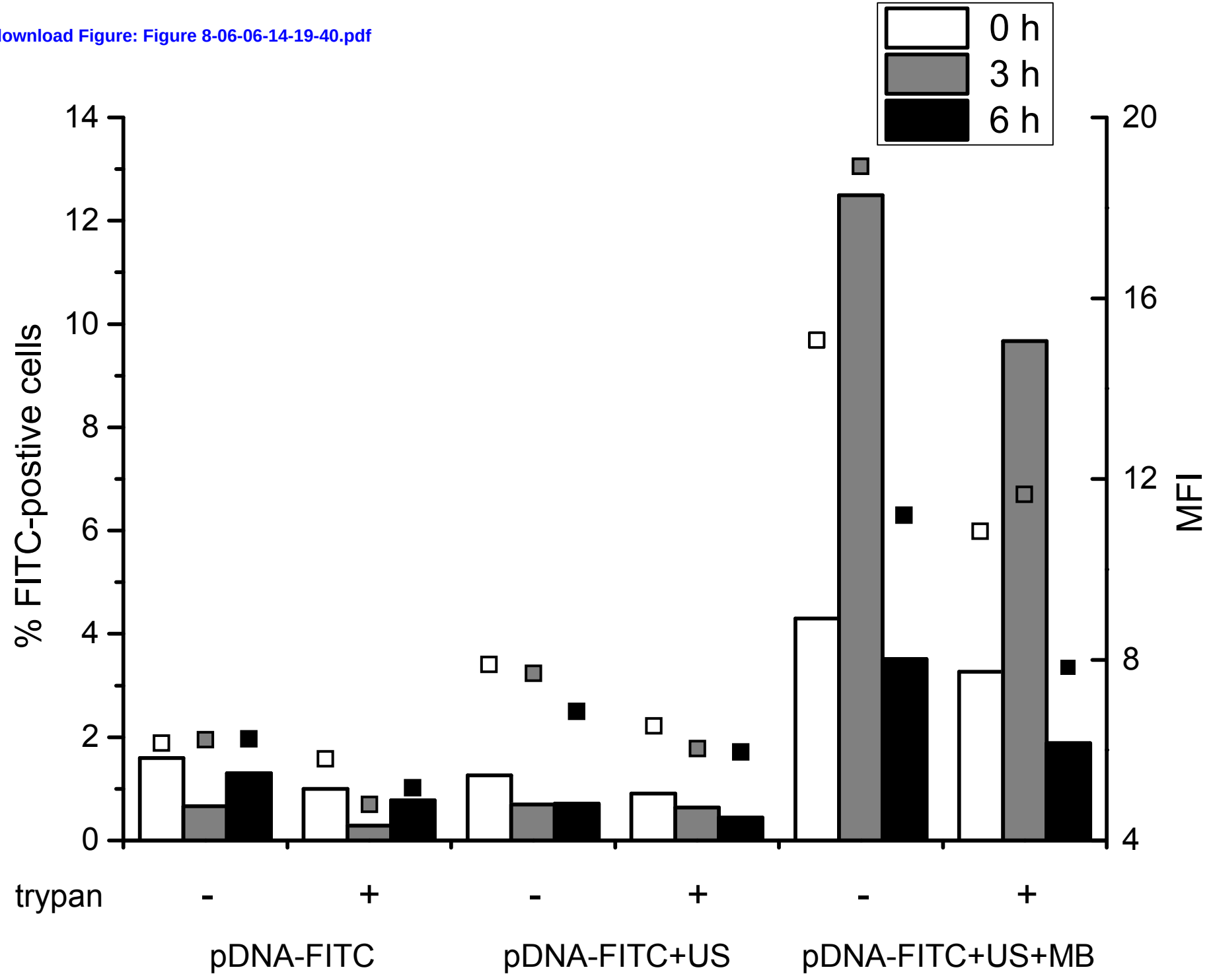

Figure 9

Click here to download Figure: Figure 9.pdf

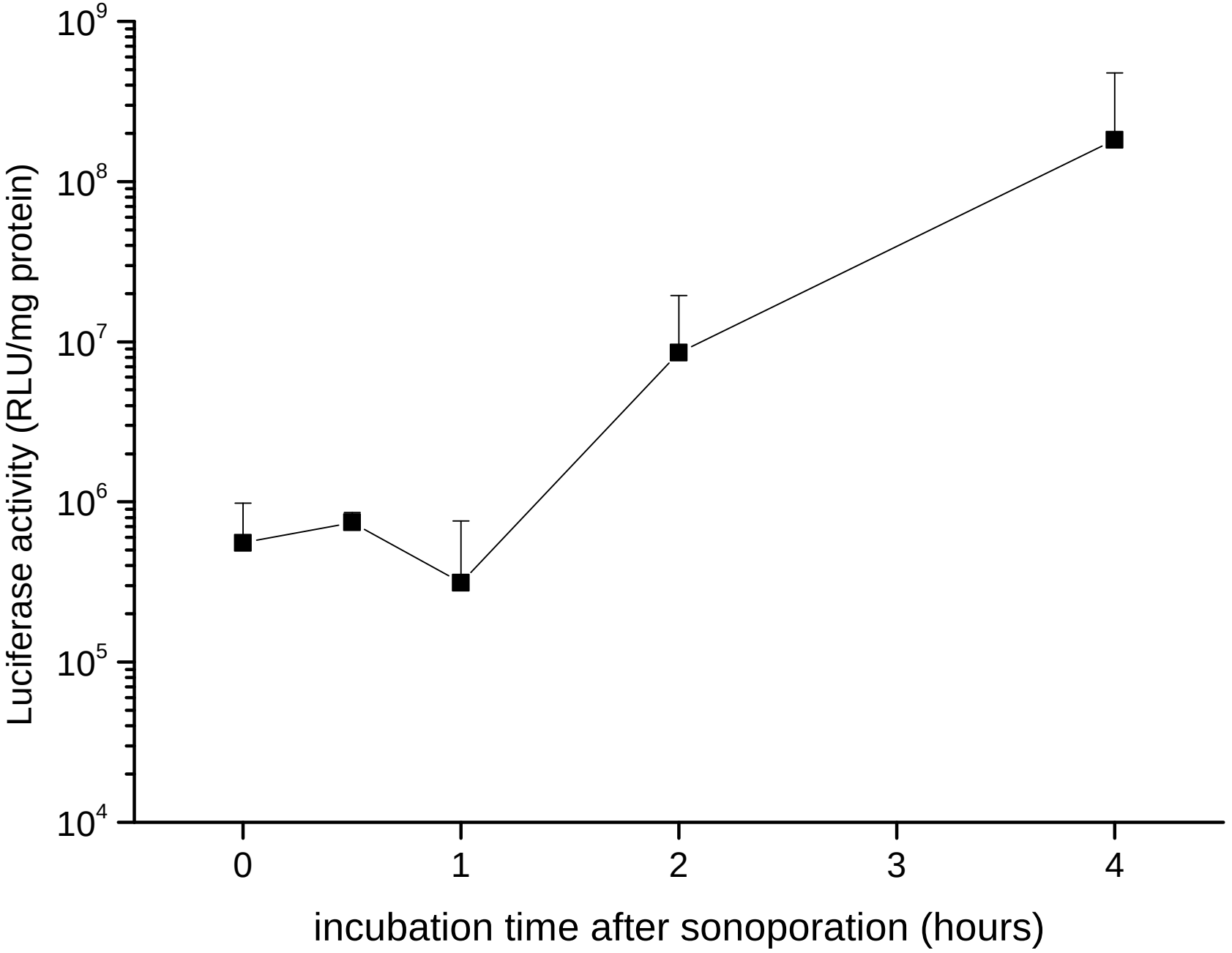

Figure 10

Click here to download Figure: figure 10.pdf

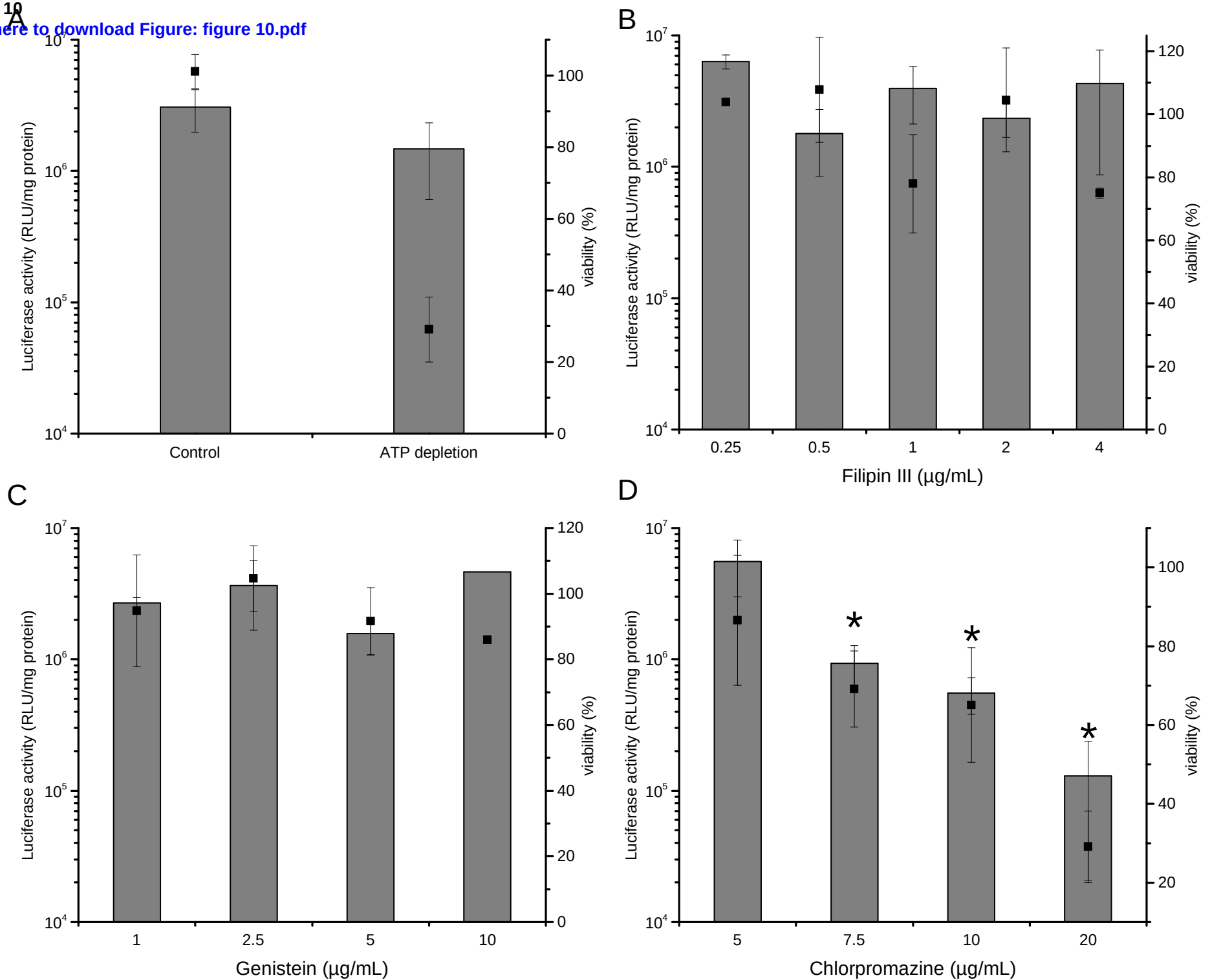

Supplemental Video

Click here to download Supplemental Video: UMB paper.mp4